

Available online at [www.sciencedirect.com](http://www.sciencedirect.com)

ScienceDirect

journal homepage: [www.elsevier.com/locate/AJPS](http://www.elsevier.com/locate/AJPS)

Original Research Paper

# Effect of Kupffer cells depletion on ABC phenomenon induced by Kupffer cells-targeted liposomes

Chaoyang Lai<sup>1</sup>, Cong Li<sup>1</sup>, Mengyang Liu, Qiujuan Qiu, Xiang Luo, Xinrong Liu, Ling Hu, Yihui Deng\*, Yanzhi Song\*

Shenyang Pharmaceutical University, Shenyang 110016, China

## ARTICLE INFO

## Article history:

Received 27 April 2018

Revised 2 July 2018

Accepted 20 July 2018

Available online 4 September 2018

## Keywords:

Accelerated blood clearance (ABC) phenomenon  
Kupffer cells  
Depletion  
Liposomes  
Bio-distribution

## ABSTRACT

Accelerated blood clearance (ABC) phenomenon is common in many PEGylated nanocarriers, whose mechanism has not been completely elucidated yet. In this study, the correlation between Kupffer cells (KCs) and ABC phenomenon has been studied by KCs-targeted liposomes inducing ABC phenomenon and KCs depletion. In other words, the 4-aminophenyl- $\alpha$ -D-mannopyranoside (APM) lipid derivative DSPE-PEG<sub>2000</sub>-APM (DPM), and 4-aminophenyl- $\beta$ -L-fucopyranoside (APF) lipid derivative DSPE-PEG<sub>2000</sub>-APF (DPF) were conjugated and modified on alendronate sodium (AD) liposomes to specifically target and deplete KCs. The dual-ligand modified PEGylated liposomes (MFPL) showed stronger ability to damage KCs *in vitro* and *in vivo*, which also could indirectly illustrate that dual-ligand modification could better target KCs. Besides, the hepatic biodistribution and pharmacokinetics could directly prove that MFPL had a stronger targeting ability to KCs. In addition, in depletion rats, plasma concentration and splenic biodistribution of MFPL and PEGylated liposomes (PL) were significantly elevated and hepatic biodistribution was significantly reduced, which demonstrated that KCs played an important role on elimination of nanoparticles. What's more, ABC phenomenon of the secondary injection of PL was stronger in KCs depletion rats than that in normal rats, which indicated that depletion of KCs prolonged the circulation of PL in the first injection repeatedly stimulating B-cells in the marginal region of the spleen and causing it to secrete more IgM antibodies. This could also illustrate that anti-PEG IgM takes up a major station compared with KCs. Most important of all, KCs-targeted liposomes could induce a stronger ABC phenomenon than PL in normal rats, which declared that based on the same IgM concentration, the more the KCs were stimulated, the stronger ABC phenomenon was induced. However, in depletion rats, this difference of ABC phenomenon between PL and MFPL could no more exist, further demonstrating that KCs could participate and play a certain role in the ABC phenomenon.

© 2018 Published by Elsevier B.V. on behalf of Shenyang Pharmaceutical University.

This is an open access article under the CC BY-NC-ND license.

(<http://creativecommons.org/licenses/by-nc-nd/4.0/>)

\* Corresponding authors. Shenyang Pharmaceutical University, No.103, Wenhua Road, Shenyang 110016, China. Tel.: +86 24 43520553. E-mail addresses: [dengyihui@syphu.edu.cn](mailto:dengyihui@syphu.edu.cn) (Y. Deng), [songyanzhi@syphu.edu.cn](mailto:songyanzhi@syphu.edu.cn) (Y. Song).

<sup>1</sup> Both authors contributed equally to this work.

Peer review under responsibility of Shenyang Pharmaceutical University.

<https://doi.org/10.1016/j.ajps.2018.07.004>

1818-0876/© 2018 Published by Elsevier B.V. on behalf of Shenyang Pharmaceutical University. This is an open access article under the CC BY-NC-ND license. (<http://creativecommons.org/licenses/by-nc-nd/4.0/>)

## 1. Introduction

Accelerated blood clearance (ABC) phenomenon is common in many PEGylated pharmaceutical preparations, which changes the pharmacokinetics and biodistribution of the subsequently injection of PEGylated nanoparticles. The universally accepted mechanism of ABC phenomenon is indicated below [1–3]: Primarily administered PEGylated nanoparticles serve as TI-2 antigens, which would stimulate B cells in marginal zone of spleen in the induction phase. Then anti-PEG IgM were secreted and supposed to accelerate elimination of nanoparticles in the secondary injection from blood.

However, the reason of ABC phenomenon induced by PEGylated nanoparticles has not been fully illuminated. Ishida et al. reported that splenectomy failed to completely eliminate the rapid clearance and enhanced hepatic accumulation of PEGylated liposomes [4]. Wang et al. also reported that ABC phenomenon was existent even in rats pretreated with conventional liposomes which were not TI-2 antigens [5]. Wang et al. reported that in rats of which complement had been depleted, the ABC phenomenon was not entirely eradicated [6]. Hence, in addition to the acquired immunity, there are other contributors can induce the ABC phenomenon. Kupffer cells (KCs), which are important cellular components of the innate immune system, are considered to be largely responsible for cellular uptake of nanoparticles in the liver [7]. KCs, as a type of antigen-presenting cells (APCs), provide a bridge between the innate and adaptive immune systems. In previous studies, we found that KCs-targeted liposomes could induce a stronger ABC phenomenon than PL in normal rats, which preliminarily proved the role of KCs in ABC phenomenon [8]. In this study, we further explored the effects of KCs depletion on the ABC phenomenon.

Bisphosphonates liposomes were reported to be used to deplete macrophage, on account of the liposome-mediated endocellular delivery of the bisphosphonate clodronate [9,10] in previous study. Liposomes serve as Trojan horses to introduce the small bisphosphonates molecules into cells. Once uptake by cells, the phospholipid bilayers of liposomes are destroyed by lysosomal phospholipases. The hydrophilic bisphosphonates molecules released inside cells could not get away from the cell, due to they could not easily traverse its cytomembranes. When more liposomes are uptake and digested, the intracellular bisphosphonates concentration rapidly increases. As a result, at a certain bisphosphonates concentration, irreversible damage will occur and promote macrophage apoptosis [11,12]. Alendronate sodium (AD) liposomes was demonstrated to be a better preparation to deplete macrophage than clodronate liposomes in previous study [13–15].

Mannose/fucose derivatives were widely applied to target mannose/fucose receptors [16–18], mannose/fucose receptors were widely expressing on the membrane of KCs [19,20]. In our previous study, the 4-aminophenyl- $\alpha$ -D-mannopyranoside (APM) lipid derivative DSPE-PEG<sub>2000</sub>-APM (DPM), and 4-aminophenyl- $\beta$ -L-fucopyranoside (APF) lipid derivative DSPE-PEG<sub>2000</sub>-APF (DPF) were synthesized and modified on liposomes, which were proved to be an efficient carrier for targeting KCs [8]. In this study, DPM/DPF was modified on AD-loaded liposomes to obtain the AD-MFPL, which showed

stronger ability to deplete KCs both *in vitro* and *in vivo*. Effect of Kupffer cells depletion on ABC phenomenon induced by PEGylated liposomes (PL) and dual-ligand modified liposomes (MFPL) was respectively evaluated by examining the pharmacokinetics and biodistribution of liposomes. The results indicated that KCs played an important role on elimination of nanoparticles and KCs could also play a certain role in the ABC phenomenon although the anti-PEG IgM took up a major station compared with KCs. This study concerned about the role of innate immune cells (KCs) in the ABC phenomenon and offered a complement for the classical mechanism of the ABC phenomenon.

## 2. Materials and methods

### 2.1. Materials

4-Aminophenyl- $\alpha$ -D-mannopyranoside (APM) and 4-aminophenyl- $\beta$ -L-fucopyranoside (APF) were purchased from Aladdin Bio-Chem Technology Co., Ltd. (Shanghai, China). 3-(N-Succinimidylxyglutaryl)-aminopropyl, polyethyleneglycol2000, carbamylidistearoyl-phosphatidylethanolamine (DSPE-PEG<sub>2000</sub>-NHS), and N-(carbonyl-methoxy polyethylene glycol-2000)-1,2-distearoyl-sn-glycero-3-phosphoethanolamine (mPEG<sub>2000</sub>-DSPE) were obtained from Shanghai Advanced Vehicle Technology Pharmaceutical, Ltd. (Shanghai, China). Hydrogenated soy phosphatidylcholine (HSPC) was obtained from Lipoid (Ludwigshafen, Germany). Cholesterol (CH) was purchased from Genzyme Corporation (Cambridge, MA, USA). Alendronate sodium (AD) was obtained from Beijing HWRK Chem Co., Ltd. (Beijing, China). Cell Counting Kit 8 (CCK8) was purchased from Dojindo (Japan). 1,1'-dioctadecyl-3,3',3'-tetra-methylindotricarbocyanine iodide (DiR) was purchased from Molecular Probes Inc. (Eugene, OR, USA). Sephadex G50 was purchased from Pharmacia Biotech Inc. (Piscataway, NJ, USA). Collagenase IV was purchased from Sigma Aldrich Chemical Co., Ltd. (St. Louis, MO). D-Hank's solutions, 100- $\mu$ m cell strainer and 23 G butterfly needle (wings cut) were purchased from Dalian Melun Biotechnology Co., Ltd. (Dalian, China). Anti-CD163 PE and IgG<sub>1</sub> PE were purchased from Serotec (Oxford, UK).

### 2.2. Cells and animals

KCs were obtained from Guangzhou Jennio Biotech Co., Ltd. (Guangzhou, China). Male Wistar rats weighing 180–200 g were obtained from Liaoning Changsheng Biotechnology Co., Ltd (Benxi, China).

### 2.3. Synthesis of DPM and DPF

DPM and DPF were synthesized as described in Fig. 1. In brief, APM/APF and DSPE-PEG<sub>2000</sub>-NHS (molar ratio 10:1) were dissolved in newly distilled N,N-Dimethylformamide (DMF). The mixture was agitated for 24 h at room temperature. The resulting DPM and DPF was depurated by dialysis against purified

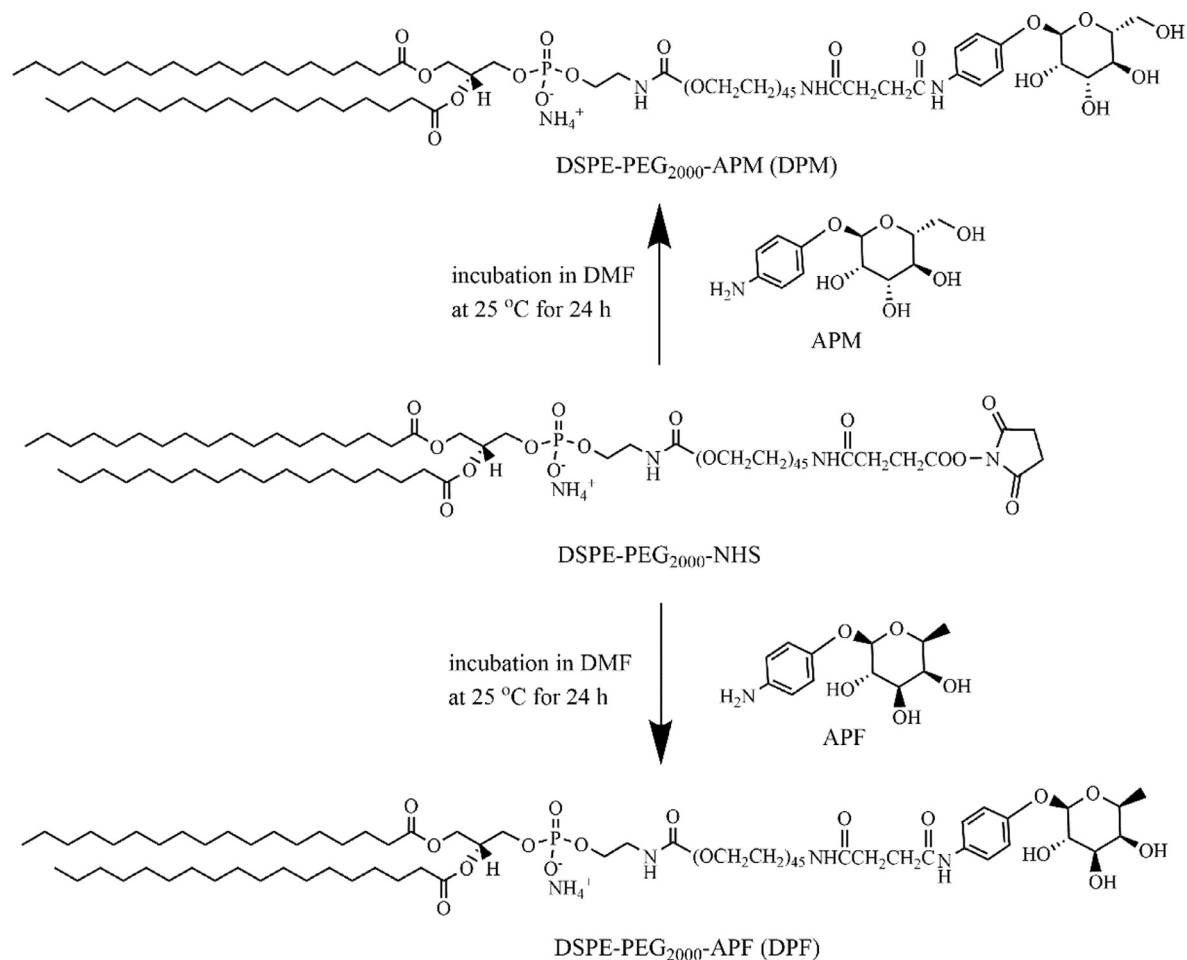


**Fig. 1. – The scheme of DPM and DPF synthesis.**

water using a dialysis bag of 1 kDa MWCO to remove the unreacted APM/APF, subsequently analyzed by <sup>1</sup>H NMR (Bruker 600 MHz).

#### 2.4. Preparation of liposomal AD

Liposomes were prepared by the lyophilization hydration method [21]. In brief, liposomes were prepared with HSPC, CH, DPM and DPF at a molar ratio of 6:2:1:1. Liposomes were dissolved in t-butanol and lyophilized overnight. The lyophilized cake was hydrated with an aqueous solution containing AD at 65 °C for 30 min with rapid stirring. The suspension was then extruded three times through polycarbonate membranes (Nucleopore, CA, USA) of 0.8, 0.4 and 0.2 μm pore sizes by means of a thermos barrel extruder (Northern Lipids, Inc., Vancouver, Canada). The obtained liposomes were purified by dialysis method. The liposomes were placed into a dialysis bag with a cut-off molecular weight (MW) of 8000 Da and dialyzed against 5% glucose solution for 24 h to remove the free AD.

#### 2.5. Characteristics of liposomal-AD

##### 2.5.1. Detection of encapsulation efficiency (EE%)

After AD loading, the AD-loaded liposomes were taken and the free AD was eliminated by Sephadex G-50 chromatogra-

phy. And then the EE% was calculated by ratio of liposomal AD and total AD content. In brief, 100 μl of the samples were loaded onto a Sephadex G50 microcolumn subsequently eluted by purified water. AD content was assessed by spectrophotometric assay of their complex with Cu<sup>2+</sup> at λ = 240 nm [22].

##### 2.5.2. Particle size distribution and zeta-potential

The Particle size distribution and zeta-potential of the AD-loaded liposomes were determined by a NICOMP™ 380 sub-micron particle analyzer (Particle Sizing System, CA, USA).

##### 2.5.3. Morphology of liposomes

The morphology of AD-loaded liposomes was observed by transmission electron microscopy (TEM) [23]. Formulations were diluted with purified water and placed on a formvar-coated copper grid (300-mesh, hexagonal fields). The samples were air-dried at 25 °C followed by removing redundant preparations. Afterwards, liposomes were adhered to the copper grid and phosphotungstic acid was used to negative stain. At last the sample was allowed to air-dry overnight at room temperature before measurement.

## 2.6. *In vitro* release of AD from liposomes

The rate at which AD was released from liposomes was measured as a function of time when the liposomes were placed into dialysis bags (10 kDa MWCO) and dialyzed against 5% glucose solution when incubated in an orbital shaker at 37 °C [24]. At various time points of 30, 60, 120, 240, 360, 480, 720, 1440, 2160, 2880 min, 0.5 ml of release medium was removed and replaced with fresh 5% glucose solution. AD content of the release media were assessed by spectrophotometric assay of their complex with  $\text{Cu}^{2+}$  at  $\lambda = 240 \text{ nm}$  [22].

## 2.7. *In vitro* cellular toxicity of liposomal AD

*In vitro* cytotoxicity of AD liposomes was evaluated by CCK8 assay. In brief, KC cells were plated at a cell density of  $5 \times 10^4$  cells/well into 96-well plates. After 12 h adherence, KCs were respectively incubated with 10  $\mu\text{l}$  different AD liposomes with AD concentrations ranging from 1 to 100  $\mu\text{M}$  for 24 h. And then cells were incubated with 10  $\mu\text{l}$  CCK8 solution for an additional 2 h. The absorbance was measured at 450 nm using a Microplate reader-SpectraMax M3 (Molecular Devices Instrument Co., Ltd., US). The half maximal inhibitory concentrations ( $\text{IC}_{50}$ ) were calculated to comparing the cytotoxicity of various AD-loaded preparations.

## 2.8. Amounts of KCs in liver after depletion

Rats were administered AD liposomes intravenously (via the tail vein) at 10 mg/kg to deplete KCs [25,26]. After 48 h, amounts of KCs in liver after depletion were detected by flow cytometry. In brief, liver cells suspensions were prepared by *in situ* liver perfusion method [27]. Rats were anesthetized by 10% chloral hydrate and sterilized by 70% ethanol solution. The abdominal cavity was cut through, and then the portal vein and inferior vena cava were exposed. A 23 G butterfly needle (wings cut) was cannulated into the portal vein. The lower part of the inferior vena cava was incised after 2 ml D-Hank's solution perfusion. D-Hank's solution was kept on being perfused with a flow rate at 7 ml/min. After 15 min of D-Hank's perfusion, 0.05% collagenase IV solution was perfused for 10 min with a flow rate at 10 ml/min. Then the liver was removed from the abdominal cavity. Liver cell suspensions were doused from liver using PBS solution and filtered through a 100- $\mu\text{m}$  cell strainer. Liver cell suspensions were centrifuged at 1000 rpm for 5 min and then diluted into a concentration of  $1 \times 10^6$  cells/ml. KCs of liver cell suspensions was stained for 30 min at 4 °C in the dark by anti-CD163 PE. Liver cell suspensions were washed thrice by PBS. Fluorescent character of cells was detected by flow cytometry.

## 2.9. Pharmacokinetics and bio-distribution of liposomes in KCs depletion rats

### 2.9.1. Pharmacokinetic studies of a single intravenous injection of liposomes

To determine the effect of KCs depletion on clearance of liposomes, a pharmacokinetic study of a single intravenous injection of PEGylated liposomes was performed on male

Wistar depletion rats and normal rats. Depletion rats were established by administered AD liposomes intravenously (via the tail vein) at 10 mg/kg. Pharmacokinetic studies were performed on depletion rats at 48 h after AD-MFPL injection.

Briefly, depletion rats and normal rats (as control) were respectively divided into two groups (3 rats per group) and intravenously administrated with DiR-PL and DiR-MFPL at a dose of 0.65 mg DiR/kg. At various time points of 0.017, 0.083, 0.25, 0.5, 1, 4, 8, 12, 24 h after injection, 0.5 ml blood were obtained through the orbital sinus and placed into microcentrifuge tubes pretreated with anticoagulant sodium heparin. Blood was centrifugated (4500 rpm, 10 min) to prepare plasma. The plasma was mixed with ethanol and then centrifugated at 10 000 rpm for 10 min. Next, the supernatant (200  $\mu\text{l}$ /well) was added into a 96-well plate and measured photometrically on the Microplate Reader-SpectraMax M3 with excitation/emission wavelengths at 750/790 nm, respectively.

### 2.9.2. Pharmacokinetics of subsequently injected PEGylated liposomes

To study the effect of KCs depletion on ABC phenomenon induced by KCs-targeted liposomes, KCs-targeted liposomes MFPL was used in a single intravenous injection in depletion rats and normal rats. In other words, the depletion rats were intravenously injected blank MFPL and PL at 15  $\mu\text{mol}$  phospholipids/kg for the first administrated (normal rats, as control, were dealt with the same procedure). After 7 d, all groups were injected intravenously with DiR-PL at the same dosage. At specified time point after administrated, blood samples (0.5 ml) were collected and processed using the same procedure described in 2.9.1.

### 2.9.3. Bio-distribution of liposomes in KCs depletion rats

After all blood samples were collected at specific time points, the rats of all group were euthanized, and livers and spleens were dissected and washed in 0.9% NaCl solution. Tissue samples were treated as follows: 200  $\mu\text{l}$  of homogenates (equivalent to 0.1 g tissue) were mixed with ethanol (800  $\mu\text{l}$ ). The entire mixture was vortexed for 5 min and centrifuged at 10 000 rpm for 10 min. The supernatant (200  $\mu\text{l}$ /well) was added into a 96-well plate and measured photometrically on the Microplate Reader-SpectraMax M3 at excitation 750 nm/emission 790 nm to determine the bio-distribution of liposomes in different organs.

## 2.10. Detection of anti-PEG IgM antibodies [2]

mPEG<sub>2000</sub>-DSPE ethanol solution (0.56 mg/ml) was added into a 96-well plate (50  $\mu\text{l}$ /well). After dried under 25 °C, the plate was blocked by 100  $\mu\text{l}$  1% BSA solution (dissolved in Tris-buffer). Every well was washed three times with 0.1% BSA Tris-buffer after 1 h blocking. Then the serum collected from rats was diluted 100 folds with Tris-buffer containing 1% BSA. Diluted serum was added into 96 wells and incubated for 1 h. Every well needed to be washed five times after 1 h incubation. Then horseradish peroxidase conjugated goat anti-rat IgM (Bethyl Laboratories Inc., TX, USA) was added into the 96-well plate (100  $\mu\text{l}$ /well) at a concentration of 1  $\mu\text{g}/\text{ml}$ . The plate

**Table 1. – Composition and characters of liposomal-AD (n = 3).**

Formulation	Liposomal composition (w/w)	Size (nm)	Zeta potential (mV)	Encapsulation efficiency (%)
AD-PL	HSPC/CH/mPEG <sub>2000</sub> -DSPE (6.0/2.0/2.0)	202.5 ± 11.3	-24.7 ± 3.9	22.6 ± 0.9
AD-MFPL	HSPC/CH/DPM/DPF (6.0/2.0/1.0/1.0)	209.0 ± 7.9	-25.0 ± 1.9	22.5 ± 1.7

was performed as before, which was washed five times after 1 h incubation. 1 mg/ml O-phenyldiamine solution was added into each well and incubating for 15 min. Next, 2 M H<sub>2</sub>SO<sub>4</sub> was used to stop the reaction when it was added into the 96-well plate (100 µl/well). Absorbance was determined at 490 nm by Microplate reader-SpectraMax M3.

### 2.11. Statistical analysis

Statistical difference was calculated by Student's t-test with SPSS software. P values was applied to Statistical differences. P < 0.05 was considered statistically significant. P < 0.01 was considered statistically extremely significant.

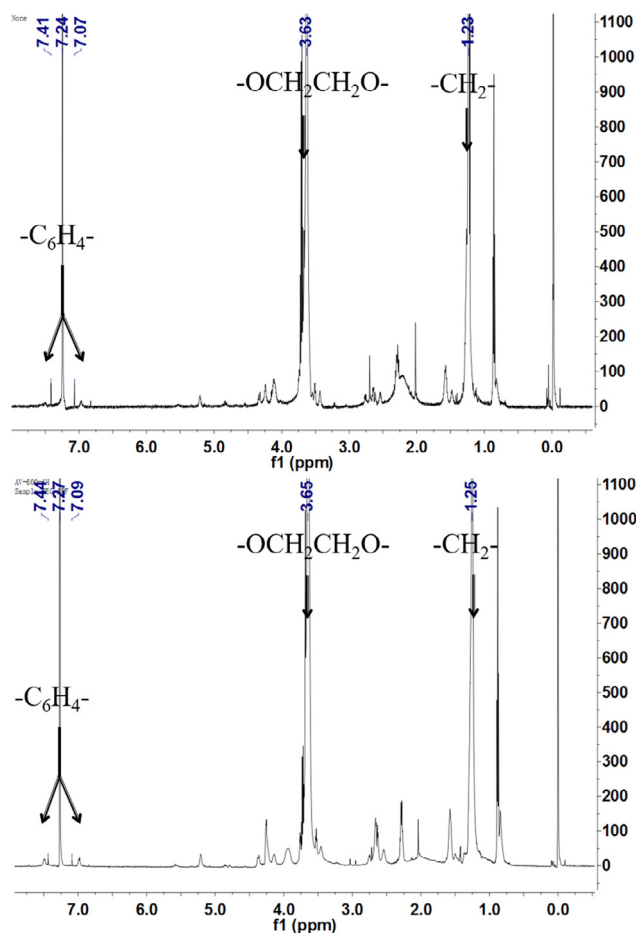
## 3. Results and discussion

### 3.1. Synthesis and characterization of DPM and DPF

DPM and DPF were synthesized as described [8]. The process of DPM and DPF syntheses was shown in Fig. 1. <sup>1</sup>H NMR was used to characterize the structure of DPM and DPF (Fig. 2). <sup>1</sup>H NMR of DPM (CCl<sub>3</sub>D, δppm): 7.24 (s, CCl<sub>3</sub>D), 7.41, 7.07 (d, -C<sub>6</sub>H<sub>4</sub>-, p-substituted phenyl, APM), 3.63 (s, -OCH<sub>2</sub>CH<sub>2</sub>O-, PEG), 1.23 (s, -CH<sub>2</sub>-, DSPE). <sup>1</sup>H NMR of DPF (CCl<sub>3</sub>D, δppm): 7.27 (s, CCl<sub>3</sub>D), 7.44, 7.09 (d, -C<sub>6</sub>H<sub>4</sub>-, p-substituted phenyl, APF), 3.65 (s, -OCH<sub>2</sub>CH<sub>2</sub>O-, PEG), 1.25 (s, -CH<sub>2</sub>-, DSPE). As the characteristic peaks of DPM/DPF, benzene ring structure, PEG structure and DSPE structure simultaneously appeared in Fig. 2, which proved that DPM/DPF was successfully synthesized.

### 3.2. Characterizations of the liposomal-AD

Studies showed that numerous factors can make a great influence on the *in vivo* behavior of liposomes, hence characterizations of liposomes are essential [28]. Table 1 summarized some significant physicochemical properties of the AD-loaded liposomes. These results indicated that the particle sizes of the prepared liposomes were about 200 nm, and that the zeta potentials varied between -20 and -30 mV. The encapsulation efficiencies of AD in the prepared liposomes were about 20%. The morphology of formulations was further characteristic by TEM (Fig. 3). As shown in Fig. 3, AD-PL and AD-MFPL displayed a subglobose shape with the representative structure of a phospholipid bilayer, which were consistent with previous study [29,30]. The liposomes were homogeneous in size and were slightly aggregated because of the evaporation of moisture during the course of preparation of the sample.

**Fig. 2. – <sup>1</sup>H NMR spectra of DPM (up) and DPF (bottom).**

### 3.3. In vitro release assay

The *in vitro* AD retention characteristic by different formulations was investigated using the dialysis method. As shown in Fig. 4, the release of the AD from the nanoparticles was biphasic; a typical burst release phase was followed by a slower release phase AD solution could completely permeate through the dialysis bag within 8 h, whereas all liposomal formulations had a comparative small amount of AD leakage against the dialysis bag. Therefore, liposome can be used as a reservoir for drugs. There was no obvious difference in AD retention properties between AD-PL and AD-MFPL in 48 h. This result suggested that DPM and DPF co-modified liposomes (AD-MFPL) possess the same stable drug retention characteristics as AD-PL.

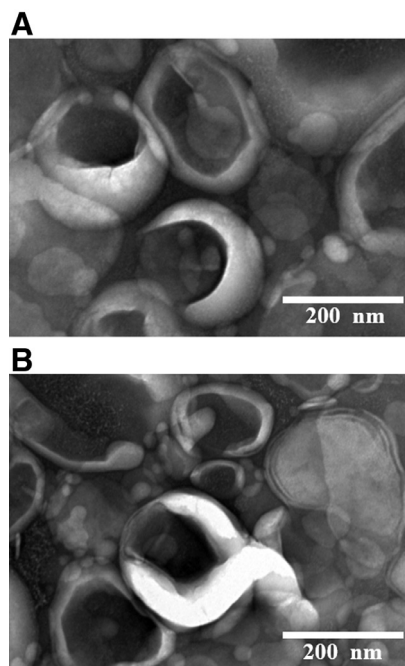


Fig. 3. – Representative TEM graphs of (A) AD-PL (B) AD-MFPL. Note: Scale bar = 200 nm.

### 3.4. In vitro cytotoxicity (CCK8) assay

The cytotoxicity of the AD-loaded liposomes was tested in KC cells. For the various AD preparations, the cell viability became lower when the dose of AD increased. The  $IC_{50}$  values of the various preparations were represented in Table 2. AD-MFPL showed a lower  $IC_{50}$  compared with AD-PL, indicating that AD-MFPL exhibited stronger inhibited effect than AD-PL (Fig. 5), suggested that the modification of DPM and DPF on the phospholipid bilayer improved the inhibition of cells by preparations compared to unmodified formulations.

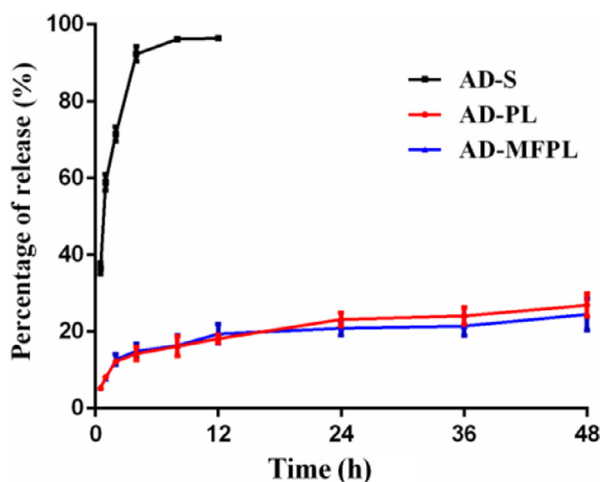


Fig. 4. – In vitro release of AD liposomes. Date represented as mean  $\pm$  SD ( $n = 3$ ).

Table 2. – The  $IC_{50}$  values of different AD liposomes on KCs.

Formulation	AD-PL	AD-MFPL
$IC_{50}$ ( $\mu$ M)	$50.96 \pm 1.06$	$23.12 \pm 0.83$

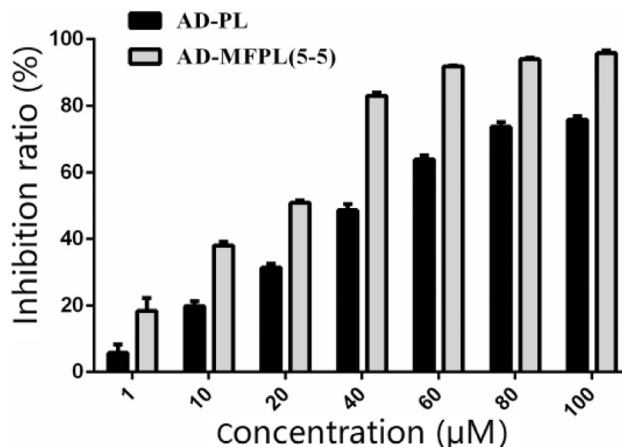


Fig. 5. – The inhibition ratio of different AD liposomes on KCs. Each value represented mean  $\pm$  SD,  $n = 6$ .

### 3.5. Depletion of KCs

Two different AD liposomes (10 mg/kg) were used to deplete KCs. Anti-CD163 antibody was used as a fluorescence marker. Therefore, PE+ means KCs in liver. PE– means other cells in liver. And amounts of KCs in liver cells suspension was evaluated by flow cytometry. The relative ratio of KCs in liver cell suspension compared with controls decreased from 19.4% to 8.19% and to 3.76%, when AD-PL and AD-MFPL were administered respectively (Fig. 6).

When the AD-MFPL was applied, 80% KCs in the liver were depleted (Fig. 6D). These results directly showed that the modification of DPM/DPF on the lipid bilayer can increase the specific uptake of liposomes by KCs. This may be attributed to the fact that the surface of KCs could express high level of mannose receptor [19,20]. The established depletion rat model was used to determine the influence of KCs depletion on ABC phenomenon in the following experiment.

### 3.6. Effect of KCs depletion on ABC phenomenon

#### 3.6.1. Effect of KCs depletion on pharmacokinetic and bio-distribution of a single intravenous injection of liposomes

To study the targeting ability of MFPL and effect of KCs depletion on a single intravenous injection of liposomes, DiR was applied as fluorescence probe to label liposomes, so as to examine the bio-distribution and pharmacokinetics studies. In other words, bio-distribution and pharmacokinetics studies of PL and MFPL were performed on Wistar rats before and after depletion, respectively.

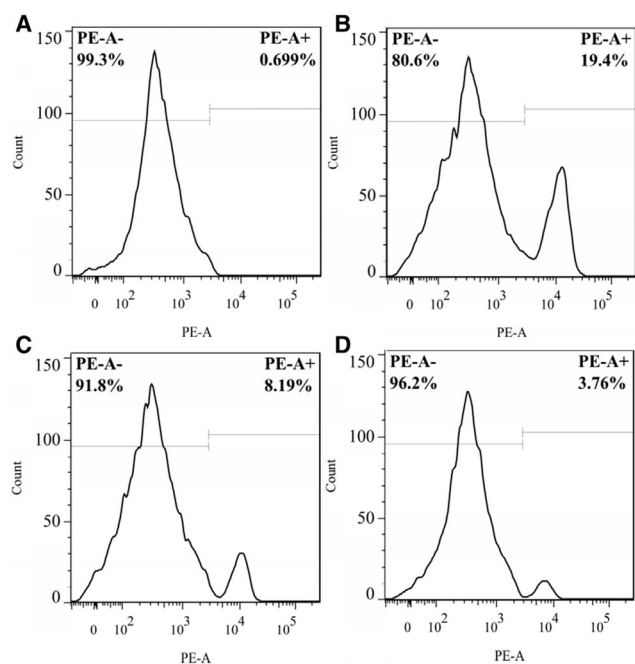


**Fig. 6.** – The relative ratio of KCs in liver cells suspension in vivo at 48 h after AD injection. (A) Rat was administered normal saline intravenously. Live cells suspension was incubated with isotype as negative control. (B) Rat was administered normal saline intravenously. Live cells suspension was incubated with anti-CD163 PE. (C) Rat was administered AD-PL intravenously. Live cells suspension was incubated with anti-CD163 PE. (D) Rat was administered AD-MFPL intravenously. Live cells suspension was incubated with anti-CD163 PE.

In normal rats, MFPL, compared with PL, showed a higher accumulation in liver ( $P < 0.01$ ), which directly proved that MFPL had a stronger targeting ability to KCs (Fig. 7B). When KCs were not depleted, a significantly difference in DiR concentration versus time curves was obvious for PL and MFPL (Fig. 7A). This is due to that DiR-MFPL had stronger ability to target KCs in the liver and therefore cleared more quickly from the blood.

However, in the rats depleted of KCs, the clearance rate of both liposomes was slower in vivo, which further illustrated that KCs played an important role on clearance of nanoparticles in liver [7]. In another study, Tsoi et al. [31] showed that, the flow rate of the nanomaterials slows by 1000 times in the liver to increase interaction and uptake by KCs. In addition, there was no significant difference between the dual ligand modified liposomes and the ordinary liposomes when the drug-time curve of the two was compared in depletion rats (Fig. 7A). On the other hand, as shown in Fig. 7B, there was no statistic difference between the distribution in liver of MFPL and PL in depletion rats ( $P > 0.05$ ). This indicated that when KCs were depleted, the target role of dual-ligand modification was lost.

In addition, concentration of anti-PEG IgM was measured at 7 d after the first injection of PL and MFPL in depletion rats and normal rats. When IgM concentration of experiment

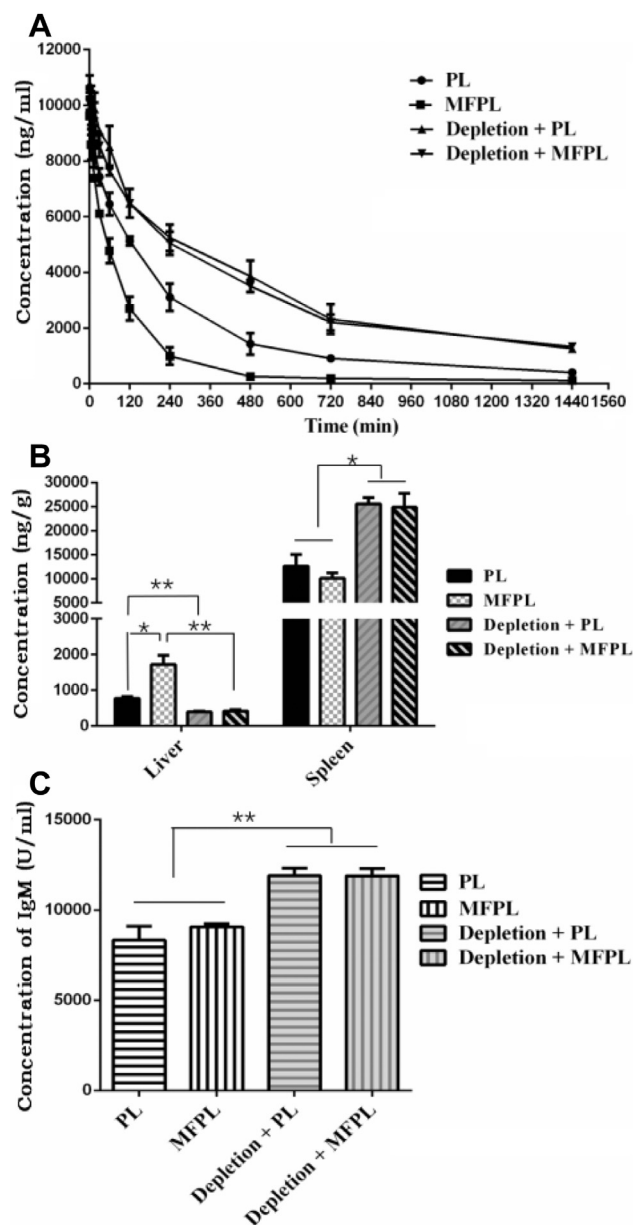


**Fig. 7.** – The effect of KCs depletion on the pharmacokinetics and biodistribution of a single intravenous injection of DiR-PL and DiR-MFPL. (A) Pharmacokinetic profile. (B) Quantitative analysis of the liver and spleen in rats 24 h after intravenous administration. (C) Determination of anti-PEG IgM at 7 d after the first injection of PL and MFPL in rats. Data are shown as mean  $\pm$  SD,  $n = 3$  (\* $P < 0.05$ , \*\* $P < 0.01$ ).

group was calculated, OD value of blank control (data not shown) was subtracted as background values. After depletion, the concentration of IgM was significantly elevated ( $P < 0.01$ ).

3.6.2. *Effect of depletion on ABC phenomenon induced by PL*  
The influence of KCs depletion on ABC phenomenon was clearly observed after seven days of the first injection of PL. ABC index was applied by Ishihara et al. [32] to assessed the

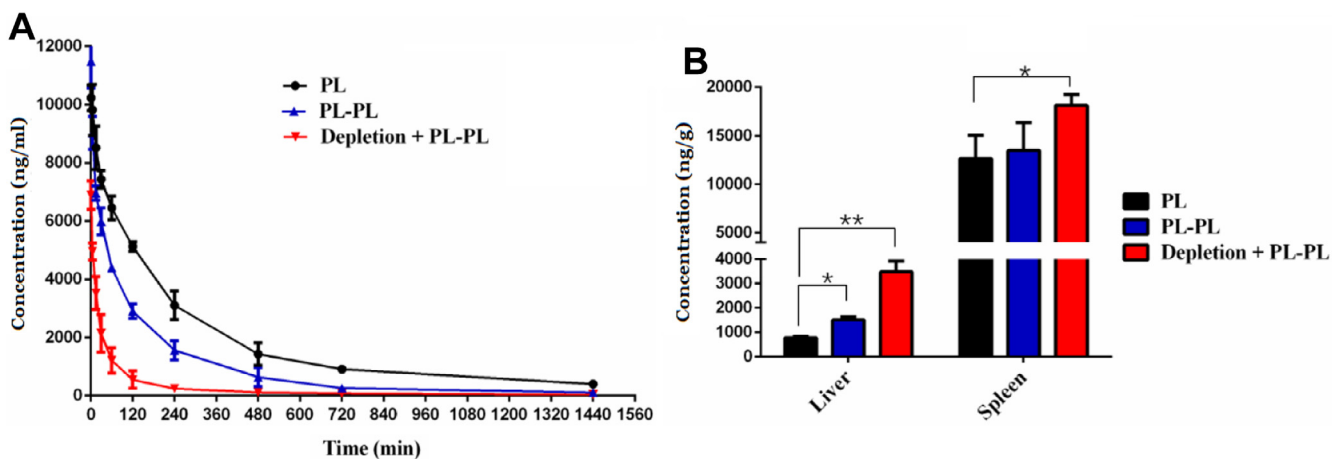


**Fig. 8.** – The effect of KCs depletion on the pharmacokinetics and biodistribution of PL induced ABC phenomenon. Depleted rats or normal rats were administered PL at a dose of 15  $\mu\text{mol}$  phospholipids/kg or 5% glucose solution. After 7 d, they were injected with PL of the test dose. (A) Pharmacokinetic profile. (B) Quantitative analysis of the liver and spleen in rats 24 h after intravenous administration. Data are represented as mean  $\pm$  SD,  $n = 3$  (\* $P < 0.05$ , \*\* $P < 0.01$ ).

**Table 3.** – The effect of KCs depletion on the ABC index of the phenomenon induced by PL and MFPL in the second dose ( $n = 3$ ).

Group	AUC <sub>(0–1 h)</sub> (mg/l·h)	ABC index <sub>(0–1 h)</sub>
PL	7.83 $\pm$ 0.30	
PL-PL	6.42 $\pm$ 0.08	0.82 $\pm$ 0.01
MFPL-PL	4.34 $\pm$ 0.82	0.55 $\pm$ 0.10
Depletion + PL-PL	2.77 $\pm$ 0.49	0.35 $\pm$ 0.06
Depletion + MFPL-PL	2.61 $\pm$ 0.66	0.33 $\pm$ 0.08

The ABC index was calculated according to the following equation:  $\text{AUC}_{(0-1 h)}$  of subsequently administration of the experimental group/ $\text{AUC}_{(0-1 h)}$  of single administration of PL.

intension of the ABC phenomenon, which was calculated by  $\text{AUC}_{(0-t)}$  of the second injection/that of the first injection.

In this experiment, the ABC index was calculated according to the following equation: the  $\text{AUC}_{(0-1 h)}$  of the subsequently injection of PL/the  $\text{AUC}_{(0-1 h)}$  of the single injection PL. A lower index indicated faster elimination of liposomes and a stronger ABC phenomenon. As shown in Fig. 8 and Table 3, whether in depletion rats or in normal rats, the first injection of PL decreased the circulation time of secondary injection of PL compared to that in the control group, which confirmed ABC phenomenon still exists in KCs depletion rats. After depletion of KCs, the first injection of PL resulted in faster blood clearance of the secondary injection of PL (Table 3). Besides, the distribution of the secondary injection of PL in liver and spleen was significantly increased in KCs depletion rats ( $P < 0.01$ ).

It was reported that anti-PEG IgM secreted by splenic marginal zone B cells was responsible for the ABC phenomenon [33,34]. Therefore, the results described above might be contributed to the fact that depletion of KCs prolonged the circulation of PL in the first injection, repeatedly stimulating B-cells in the marginal region of the spleen, causing it to secrete

more anti-PEG IgM antibodies (Fig. 7C), which in turn leads to enhancement of the ABC phenomenon. This could also illustrate that anti-PEG IgM takes up a major station compared with KCs.

### 3.6.3. Effect of depletion on ABC phenomenon induced by MFPL

As shown in Fig. 9, in normal rats and KCs depletion rats, both pretreated with PL and MFPL would induce ABC phenomenon and enhancement of hepatic and splenic accumulation, which was coincident with the conclusion in Section 3.6.2.

Interestingly, in normal rats, based on the same IgM concentration (Fig. 7C), pretreated with MFPL possessed faster blood clearance (Fig. 9A) and a higher hepatic accumulation (Fig. 9B) of the secondary injection of PL than pretreated with PL ( $P < 0.05$ ). IgM concentration suggested that splenic marginal zone B cells would not be responsible for the faster clearance of the subsequent PL injection (Fig. 7C). Pretreated with MFPL induced a stronger ABC phenomenon than pretreated with PL when ABC index was calculated (Table 3), which illustrated that based on the same IgM concentration, liposomes targeted the KCs at the first injection of MFPL, stimulated the liver more, and thus induced a stronger ABC phenomenon.

However, in KCs depletion rats, this difference of ABC phenomenon between pretreated with MFPL and PL could no more exist. The pharmacokinetics (Fig. 9C), biodistribution (Fig. 9D), and anti-PEG IgM concentration (Fig. 7C) became almost completely similar. In KCs depletion rats, PL-PL group and MFPL-PL group induce the same intension of ABC phenomenon when ABC index was calculated (Table 3). This may be due to the fact that KCs were almost completely depleted, MFPL lost its original targeting role, and showed the same in the ABC phenomenon as PL.

In summary, the ABC phenomenon “difference” between MFPL-PL and PL-PL in normal rats and the ABC phenomenon “similarity” between MFPL-PL and PL-PL in KCs depletion rats

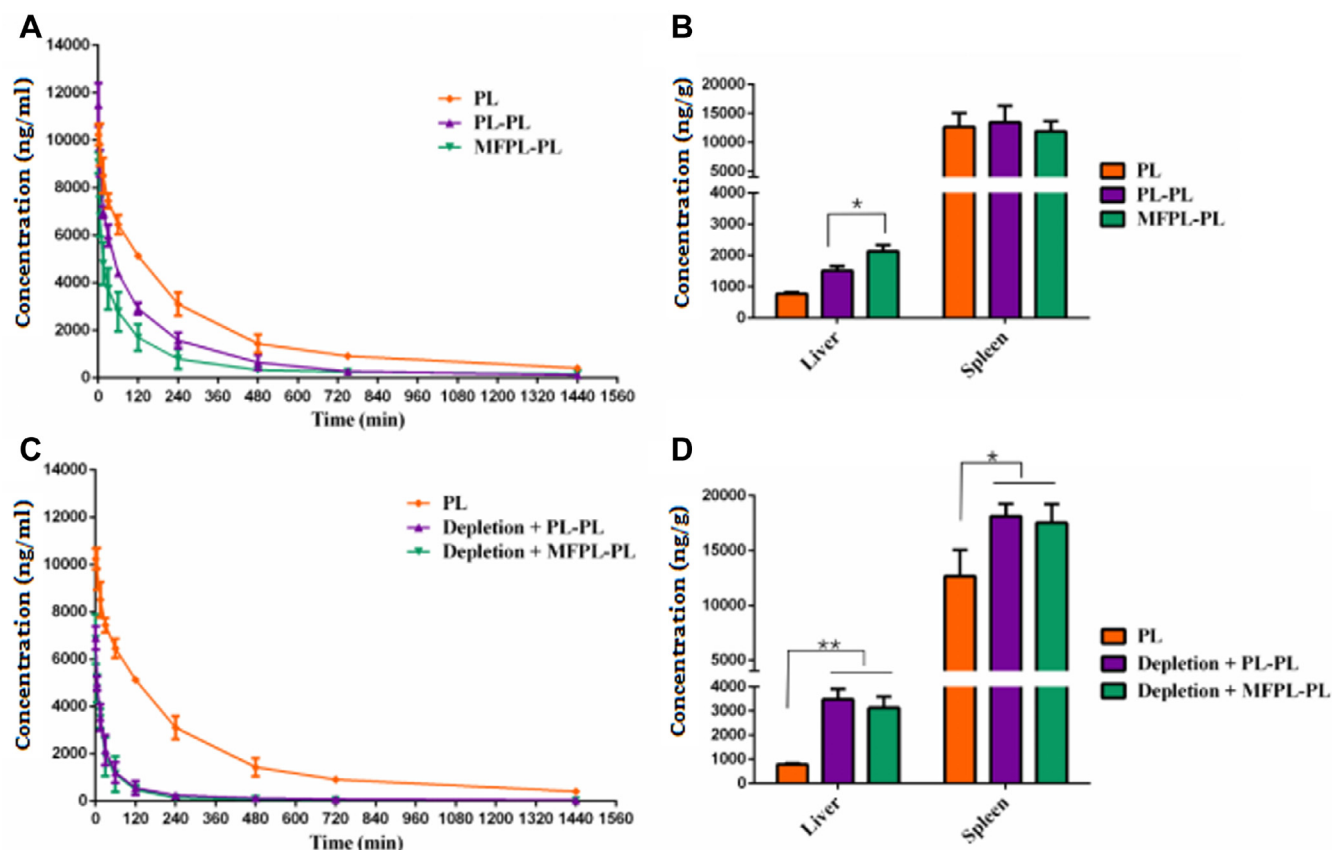


**Fig. 9.** – The effect of KCs depletion on the pharmacokinetics and biodistribution of MFPL induced ABC phenomenon. After 7 d, rats were injected with PL and MFPL at a dose of 15  $\mu\text{mol}$  phospholipids/kg. (A) Pharmacokinetic profile of MFPL in normal rats. (B) Quantitative analysis of the liver and spleen in normal rats 24 h after intravenous administration. (C) Pharmacokinetic profile of MFPL in depletion rats. (D) Quantitative analysis of the liver and spleen in depletion rats 24 h after intravenous administration. Data are represented as mean  $\pm$  SD,  $n = 3$  (\* $P < 0.05$ , \*\* $P < 0.01$ ).

demonstrated that KCs could participate and play a certain role in the ABC phenomenon.

#### 4. Conclusion

The effect besides adaptive immune system and anti-PEG IgM on ABC phenomenon was objectively existent, but no one cared about this. In this report, study of KCs depletion on single injected PEGylated liposomes demonstrated that the clearance function of KCs to PEGylated liposomes in body. Effect of KCs depletion on ABC phenomenon induced by MFPL indicated that KCs could participate and play a certain role in the ABC phenomenon. This study offers a complement for the classical mechanism of the ABC phenomenon and potentially provides direction for its solution.

#### Conflicts of interest

The authors report no declarations of interest.

#### Acknowledgments

This research was supported by the National Natural Science Foundation of China (Nos. 81373334 and 81573375).

#### Supplementary materials

Supplementary material associated with this article can be found, in the online version, at doi:10.1016/j.ajps.2018.07.004.

#### REFERENCES

- [1] Shimizu T, Ishida T, Kiwada H. Transport of PEGylated liposomes from the splenic marginal zone to the follicle in the induction phase of the accelerated blood clearance phenomenon. *Immunobiology* 2013;218(5):725–32.
- [2] Ichihara M, Shimizu T, Imoto A, et al. Anti-PEG IgM response against PEGylated liposomes in mice and rats. *Pharmaceutics* 2010;3(1):1–11.

- [3] Koide H, Asai T, Hatanaka K, et al. T cell-independent B cell response is responsible for ABC phenomenon induced by repeated injection of PEGylated liposomes. *Int J Pharm* 2010;392(1–2):218–23.
- [4] Ishida T, Ichihara M, Wang X, Kiwada H. Spleen plays an important role in the induction of accelerated blood clearance of PEGylated liposomes. *J Control Release* 2006;115(3):243–50.
- [5] Wang XY, Ishida T, Ichihara M, Kiwada H. Influence of the physicochemical properties of liposomes on the accelerated blood clearance phenomenon in rats. *J Control Release* 2005;104(1):91–102.
- [6] Wang L, Su Y, Wang X, et al. Effects of complement inhibition on the ABC phenomenon in rats. *Asian J Pharm Sci* 2017;12(3):250–8.
- [7] Gustafson HH, Holt-Casper D, Grainger DW, Ghandehari H. Nanoparticle uptake: the phagocyte problem. *Nano Today* 2015;10(4):487–510.
- [8] Lai C, Li C, Luo X, et al. Use of dual-ligand modification in Kupffer cell-targeted liposomes to examine the contribution of Kupffer cells to accelerated blood clearance phenomenon. *Mol Pharm* 2018;15(7):2548–58.
- [9] Van Rooijen N, Van Nieuwmegen R. Elimination of phagocytic cells in the spleen after intravenous injection of liposome-encapsulated dichloromethylene diphosphonate. *Cell Tissue Res* 1984;238(2):355–8.
- [10] Van Rooijen N, Sanders A. Liposome mediated depletion of macrophages: mechanism of action, preparation of liposomes and applications. *J Immunol Methods* 1994;174(1–2):83–93.
- [11] Van Rooijen N, Sanders A, van den Berg TK. Apoptosis of macrophages induced by liposome-mediated intracellular delivery of clodronate and propamidine. *J Immunol Methods* 1996;193(1):93–9.
- [12] Naito M, Nagai H, Kawano S, et al. Liposome-encapsulated dichloromethylene diphosphonate induces macrophage apoptosis *in vivo* and *in vitro*. *J Leukocyte Biol* 1996;60(3):337–44.
- [13] Van Rooijen N, Sanders A. Kupffer cell depletion by liposome-delivered drugs: comparative activity of intracellular clodronate, propamidine, and ethylenediaminetetraacetic acid. *Hepatology* 1996;23(5):1239–43.
- [14] Epstein-Barash H, Gutman D, Markovsky E, et al. Physicochemical parameters affecting liposomal bisphosphonates bioactivity for restenosis therapy: internalization, cell inhibition, activation of cytokines and complement, and mechanism of cell death. *J Control Release* 2010;146(2):182–95.
- [15] Makkonen N, Salminen A, Rogers MJ, et al. Contrasting effects of alendronate and clodronate on RAW 264 macrophages: the role of a bisphosphonate metabolite. *Eur J Pharm Sci* 1999;8(2):109–18.
- [16] Yu SS, Lau CM, Barham WJ, et al. Macrophage-specific RNA interference targeting via “click”, mannosylated polymeric micelles. *Mol Pharm* 2013;10(3):975–87.
- [17] Zhu S, Niu M, O’Mary H, Cui Z. Targeting of tumor-associated macrophages made possible by PEG-sheddable, mannose-modified nanoparticles. *Mol Pharm* 2013;10(9):3525–30.
- [18] Locke LW, Mayo MW, Yoo AD, Williams MB, Berr SS. PET imaging of tumor associated macrophages using mannose coated 64Cu liposomes. *Biomaterials* 2012;33(31):7785–93.
- [19] Stahl PD. The macrophage mannose receptor: current status. *Am J Resp Cell Mol* 1990;2(4):317–18.
- [20] Stahl PD. The mannose receptor and other macrophage lectins. *Curr Opin Immunol* 1992;4(1):49–52.
- [21] Szoka F Jr, Papahadjopoulos D. Comparative properties and methods of preparation of lipid vesicles (liposomes). *Annu Rev Bioph Bio* 1980;9(1):467–508.
- [22] King L, Vieth R. Extraction and measurement of pamidronate from bone samples using automated pre-column derivatization, high-performance liquid chromatography and fluorescence detection. *J Chromatogr B Biomed Sci Appl* 1996;678(2):325–30.
- [23] Yang T, Cui FD, Choi MK, et al. Enhanced solubility and stability of PEGylated liposomal paclitaxel: *in vitro* and *in vivo* evaluation. *Int J Pharm* 2007;338(1–2):317–26.
- [24] Yang Q, Zhang T, Wang C, Jiao J, Li J, Deng Y. Coencapsulation of epirubicin and metformin in PEGylated liposomes inhibits the recurrence of murine sarcoma S180 existing CD133<sup>+</sup> cancer stem-like cells. *Eur J Pharm Biopharm* 2014;88(3):737–45.
- [25] Danenberg HD, Golomb G, Groothuis A, et al. Liposomal alendronate inhibits systemic innate immunity and reduces *in-stent* neointimal hyperplasia in rabbits. *Circulation* 2003;108(22):2798–804.
- [26] Haber E, Afergan E, Epstein H, et al. Route of administration-dependent anti-inflammatory effect of liposomal alendronate. *J Control Release* 2010;148(2):226–33.
- [27] Berry MN, Friend DS. High-yield preparation of isolated rat liver parenchymal cells: a biochemical and fine structural study. *J Cell Biol* 1969;43(3):506–20.
- [28] Drummond DC, Meyer O, Hong K, Kirpotin DB, Papahadjopoulos D. Optimizing liposomes for delivery of chemotherapeutic agents to solid tumors. *Pharmacol Rev* 1999;51(4):691–744.
- [29] Ruozzi B, Belletti D, Tombesi A, Tosi G, Bondioli L, Forni F. AFM, ESEM, TEM, and CLSM in liposomal characterization: a comparative study. *Int J Nanomed* 2011;6:557–63.
- [30] Sun J, Song Y, Lu M, et al. Evaluation of the antitumor effect of dexamethasone palmitate and doxorubicin co-loaded liposomes modified with a sialic acid–octadecylamine conjugate. *Eur J Pharm Sci* 2016;93:177–83.
- [31] Tsoi KM, MacParland SA, Ma XZ, et al. Mechanism of hard-nanomaterial clearance by the liver. *Nat Mater* 2016;15(11):1212–21.
- [32] Ishihara T, Takeda M, Sakamoto H, et al. Accelerated blood clearance phenomenon upon repeated injection of PEG-modified PLA-nanoparticles. *Pharm Res-Dordr* 2009;26(10):2270–9.
- [33] Lila A S A, Kiwada H, Ishida T. The accelerated blood clearance (ABC) phenomenon: clinical challenge and approaches to manage. *J Control Release* 2013;172(1):38–47.
- [34] Hashimoto Y, Lila A SA, Shimizu T, Ishida T, Kiwada H. B cell-intrinsic toll-like receptor 7 is responsible for the enhanced anti-PEG IgM production following injection of siRNA-containing PEGylated lipoplex in mice. *J Control Release* 2014;184:1–8.